Sea Surface Topography Estimation with Infrared Satellite Imagery

ANDREW C. VASTANO AND ROBERT O. REID

Department of Oceanography, Texas A&M University, College Station, TX 77843

(Manuscript received 20 July 1984, in final form 30 November 1984)

ABSTRACT

Sea surface flow derived from displacements of surface patterns in sequential NOAA-6 AVHRR (11 micron band) satellite images yield coherent nonuniform distributions of velocity vectors. An analytic representation of flow over the region of the distribution is obtained by performing a least-squares regression analysis for coefficients of a streamfunction expansion that is expressed in terms of trigonometric basis functions. Sea surface topography is estimated with the streamfunction by employing a geostrophic approximation. An application is made to a portion of the Oyashio Frontal Zone in the northwestern Pacific that includes the First and Second Oyashio Intrusions and an anticyclonic eddy. A horizontal map of a local rotational perturbation property is calculated for this region as a further example of the use of the streamfunction analysis.

1. Introduction

Analyses of discretely sampled velocity fields for streamfunction representations of flow were carried out by Pritchard (1948) to obtain monthly average surface currents on basinwide scales. Streamline characterizations for flow regimes in the Caribbean Sea as well as portions of the eastern North Pacific and the Gulf of Mexico were derived from charts compiled with ship reports of surface currents. In contrast, the present interest is in single mesoscale features and mesoscale fields and requires intensive observational efforts to gather synoptic data sets applicable to flow studies. Field experiments must often employ multiplatform surveys and instrument arrays to achieve sampling densities that permit resolution of significant structural and temporal changes. Near-synoptic current data as in Hubertz *et al.* (1972) or hydrographic data as in McWilliams (1976) are essential, sampled at horizontal spatial and temporal resolutions in the orders of tens of kilometers and days. Satellite orbital characteristics and sensor resolutions provide such sampling for sea surface expressions of mesoscale phenomena with infrared, microwave and visible instrumentation. In addition to present detection and tracking applications, satellites have an enormous potential for providing quantitative dynamic information about mesoscale fields and supplementing surface-acquired observations.

Estimates of motion for mesoscale features and their gross movement have been made with infrared imagery by several investigators (e.g., Vastano and Bernstein, 1984). A more recent study (Vastano and Borders, 1984) produced a field of sea surface flow vectors for mesoscale elements on the Oyashio Front northeast of Japan. An interactive algorithm requires sequential infrared (AVHRR) (11 micron band) images and computes surface velocity vector components from user-identified displacements of sea surface temperature patterns and elapsed time. This procedure assumes that the total time rate of change of a scalar quantity depends solely on horizontal advective processes and is demonstrated to have a measured repeatability of 1–2 cm s^{-1} for successive images approximately 24 hours apart. Comparison of the velocity results with surface-acquired flow measurements made during a previous field experiment indicates a general agreement in speed and direction over a semipermanent anticyclonic eddy near the thermal ridge of the Oyashio Front. Satellite-derived vector fields of this nature suggest streamfunction estimates that are made for nonuniform vector distributions as contrasted to the uniformly distributed vector fields used by Pritchard (1948). In turn, the streamfunctions can permit assessments of sea surface topographies that are independent of microwave altimetric observation. The results reported in this paper provide a method for extracting mesoscale sea surface topography from sequential infrared images and are a step toward extrapolating altimetric topography data to mesoscale areal coverage.

2. Surface topography

The use of sequential infrared images to extract surface motion estimates (Vastano and Borders, 1984) produces a nonuniform distribution of velocity components u (+ eastward) and v (+ northward) that represent advective movements apparent in the changes of sea surface temperature patterns. The advective movements of small perturbations in the temperature pattern are estimated by an investigator using an interactive image processing algorithm. The velocity

vectors (Fig. 1) are a sample of the motion that can be considered approximately planar since vertical motions are nominally much smaller than horizontal ones. A temperature range of approximately 11°C is represented in the grey scale distribution of the image (Vastano and Bernstein, 1984). The perturbations in the frontal regions associated with the warm core eddy are defined by four degree differences. The premise is that these features are created by small-scale wave or turbulent processes, represent perturbations of otherwise smooth surface isotherms, and reveal the flow regime by their displacements. Specifically, the features are of small scale relative to the baroclinic radius of deformation. Although Rossby-like or internal gravity waves can be present, it follows that their phase speeds are much less than maximum theoretical values and are therefore regarded as slower than typical mesoscale surface currents. Diffusion, heat exchange with the atmosphere and vertical motions are assumed to produce changes of temperature much less than those induced by advective processes for sequential image time intervals. A mathematical expression of this concept can be approached through the material derivative of a scalar quantity C,

$$\frac{DC}{Dt} = \frac{\partial C}{\partial t} + \mathbf{V} \cdot \nabla C = R. \tag{1}$$

C has mean (C_0) and perturbation (C_1) components and the flow regime is composed of mean ($\mathbf{V}_0$) and perturbation ($\mathbf{V}_1$) components. Thus

$$\text{and} \qquad \begin{aligned} C &= C_0 + C_1 \\ \mathbf{V} &= \mathbf{V}_0 + \mathbf{V}_1, \end{aligned} \tag{2}$$

where $\mathbf{V}_0$ is presumed nearly parallel to contours of C_0. The mean components of C and $\mathbf{V}$ are considered to be slowly evolving relative to rapid spatial and temporal fluctuations that characterize the perturbations. The right-hand side of (1) represents processes that cause negligible changes in the scalar quantity C over the time interval between images. Expanding (1) with the components of C and $\mathbf{V}$ yields

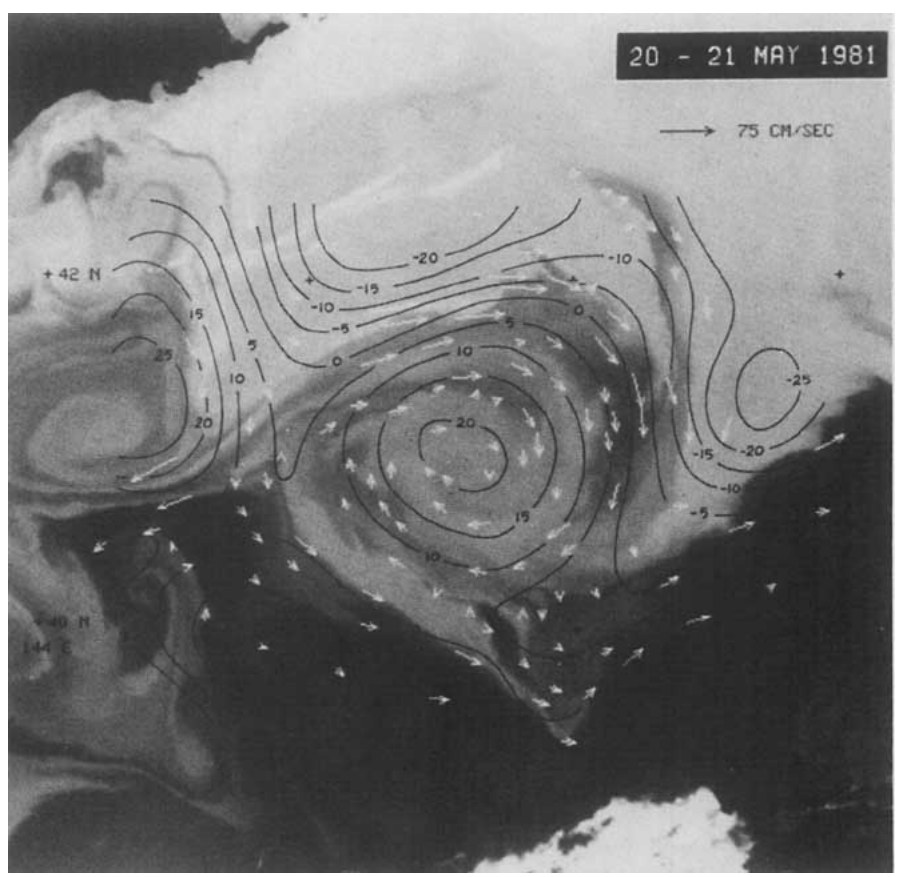

FIG. 1. Surface flow vectors from 20 and 21 May 1981 NOAA-6, AVHRR (11 micron band) images and sea surface topography overlayed on the 20 May image. Tick marks are placed at two degree latitude and longitude intervals.

$$\frac{\partial C_1}{\partial t} + \mathbf{V}_0 \cdot \nabla C_1 = S_1 + S_2, \tag{3}$$

where

$$S_1 = R - \mathbf{V}_0 \cdot \nabla C_0 - \mathbf{V}_1 \cdot \nabla C_1 - \frac{DC_0}{Dt} \tag{4}$$

$$S_2 = -\mathbf{V}_1 \cdot \nabla C_0. \tag{5}$$

Equation (4) includes the self-advective or turbulent diffusion term of the flow regime; S_1 is disregarded as a result of the short time interval. Equation (5) represents an episodic source term that gives rise to the perturbations in the scalar field. Between events, the relation

$$\frac{\partial C_1}{\partial t} + \mathbf{V}_0 \cdot \nabla C_1 = 0 \tag{6}$$

remains to relate the scalar and flow fields. The Lagrangian equivalent of (6) states that the velocities $\mathbf{V}_0$ of small water parcels are equivalent to the time rate of change of their displacements. The vectors shown in Fig. 1 are computed from such movements and are assumed to be governed by Eq. (6). When this flow is considered horizontally nondivergent, the ocean surface velocity field is derivable from a single scalar function, the streamfunction Ψ. Under an approximation of uniform Coriolis parameter, the streamfunction is proportional to the surface topography and the flow rendition is a geostrophic one.

One way of deriving Ψ from the velocity field is to interpolate the velocity data to a rectangular grid (McWilliams, 1976). This facilitates estimates of vorticity from which Ψ can be obtained by solution of Poisson's equation as in Hubertz *et al.* (1972). A simpler method is adopted here that avoids prior interpolation of the observed velocity field and minimizes the problem of specifying boundary conditions inherent in the solution of Poisson's equation. The method assumes that the field of Ψ can be represented over the data set by a series of selected basis functions in x (east), y (north). The coefficients of the series are evaluated by a least-squares fit to the velocity data by the appropriate derivatives of Ψ. Representing the streamfunction in terms of trigonometric basis functions,

$$\Psi = \sum_n \sum_m A_{n,m} \sin\frac{n\pi x}{L_x} \sin\frac{m\pi y}{L_y}, \tag{7}$$

velocity component estimates have the form

$$\tilde{u} = -\frac{\partial \Psi}{\partial y} = -\sum_n \sum_m \frac{m\pi}{L_y} A_{n,m} \sin\frac{n\pi x}{L_x} \cos\frac{m\pi y}{L_y} \tag{8}$$

$$\tilde{v} = +\frac{\partial \Psi}{\partial x} = \sum_n \sum_m \frac{n\pi}{L_x} A_{n,m} \cos\frac{n\pi x}{L_x} \sin\frac{m\pi y}{L_y}, \tag{9}$$

where the x, y coordinates are scaled by L_x and L_y, the dimensions of the rectangular region enclosing the data samples. The selection of sine terms for the streamfunction implies that Ψ vanishes on an enlarged rectangular boundary surrounding the velocity vector distribution. A least-squares error function

$$\sigma^2 = [\sum_j (\tilde{u} - u_j)^2 + (\tilde{v} - v_j)^2]/j_{\max} \tag{10}$$

over the set of observations u_j, v_j, permits a variation on the coefficients and results in a linear set of equations

$$[Z(l, k)][A(k)] = [F(l)] \tag{11}$$

for the coefficients, where k and $l = n + (m - 1)\, n_{\max}$ and

$$Z(l, k) = \sum_j [(a_l a_k)_j + (b_l b_k)_j] \tag{12}$$

$$F(l) = \sum_j (a_l u_j + b_l v_j) \tag{13}$$

and, in general,

$$a = -\frac{m\pi}{L_y} \sin\frac{n\pi x}{L_x} \cos\frac{m\pi y}{L_y} \tag{14}$$

$$b = \frac{n\pi}{L_x} \cos\frac{n\pi x}{L_x} \sin\frac{m\pi y}{L_y}. \tag{15}$$

Two constraints are added to the system that require the individual sums of $(\tilde{u} - u_j)$ and $(\tilde{v} - v_j)$ to vanish. The solution for Ψ is accomplished using standard Gauss-Jordan elimination procedures for inversion of the $Z(l, k)$ matrix. The relation of the streamfunction to sea surface topography is made by invoking a geostrophic approximation for the flow such that

$$V = \frac{\partial \Psi}{\partial s} = \frac{g}{f}\frac{\partial \eta}{\partial s}, \tag{16}$$

where f is the Coriolis parameter, g is the acceleration of gravity, and the coordinate s is taken normal to streamlines and contours of η, the sea surface topography. In this case, integration yields

$$\eta = \frac{f}{g}\Psi + \text{constant}, \tag{17}$$

where f is taken as a constant appropriate to the centroid of the data distribution.

The sea surface topography analysis constrains the satellite-observed flow components to approximate the surface relief in geostrophic terms. Clearly these components contain more information in addition to the baroclinic contribution to the flow field. The time interval between images is chosen to be short relative to the scalar changes induced by a number of mesoscale processes. However, the analysis is not comprehensive even under this selection. Wind forcing of the surface

layer has not yet been accounted for in the analysis. Such an inclusion is feasible over an image area only with wind observations at spatial and temporal resolutions comparable to the flow vector field and would require a sensor similar to the Seasat (SASS). Other dynamic mechanisms, such as centripetal acceleration, can be pertinent depending on the types of mesoscale features present in the images. Comparisons of satellite-derived velocities with surface-acquired measurements for eddies and plumes are in progress. Results of these studies will provide information relevant to the necessity for more complex analyses.

At present, a statistical measure of experimental repeatability for the topography can be quantified by considering an ensemble of possible data realizations from the same image pair that have equivalent velocity component variances. It follows from (7) and (17) that departures (η') of η from its expected value for a given x, y are

$$\eta' = \frac{f}{g} \sum_n \sum_m A'_{n,m} \sin\frac{n\pi x}{L_x} \sin\frac{m\pi y}{L_y}, \tag{18}$$

where $A'_{n,m}$ represent departures of $A_{n,m}$ from expected values for the ensemble. The expected value of the mean square deviation (MSD) for the topography is governed by

$$\sum_j \overline{(\eta'_j)^2} = \left(\frac{f}{g}\right)^2 \sum_n \sum_m \sum_p \sum_q A'_{n,m} A'_{p,q_j} \times \left(\sin\frac{n\pi x_j}{L_x} \sin\frac{p\pi x_j}{L_x} \sin\frac{m\pi y_j}{L_y} \sin\frac{q\pi y_j}{L_y}\right). \tag{19}$$

If $A'_{n,m}$ and $A'_{p,q}$ are stochastically independent realizations from an A ensemble whose variance is independent of n and m, then

$$\overline{A'_{n,m} A'_{p,q}} = \begin{cases} \overline{(A')^2}; & k = n, \quad l = m \\ 0 \quad ; & k = n \quad \text{or} \quad l = m, \end{cases} \tag{20}$$

and

$$\sum_j \overline{(\eta'_j)^2} = \left(\frac{f}{g}\right)^2 \overline{(A')^2} \sum_n \sum_m \sum_j \left(\sin^2\frac{n\pi x_j}{L_x} \sin^2\frac{m\pi y_j}{L_y}\right). \tag{21}$$

A similar analysis for deviations of the computed velocity components (u, v) gives

$$\sum_j [\overline{(u'_j)^2} + \overline{(v'_j)^2}] = \overline{(A')^2} \sum_k \sum_j (a_k^2 + b_k^2)_j = \overline{(A')^2}\, \mathrm{tr}Z. \tag{22}$$

Substitution for $\overline{(A')^2}$ in (21) yields a working relation for the expected MSD of η over the data set

$$\frac{1}{j_{\max}} \sum_j \overline{(\eta'_j)^2} = \frac{1}{\mathrm{tr}Z} \left(\frac{f}{g}\right)^2 \times \sum_n \sum_m \sum_j \left(\sin^2\frac{n\pi x_j}{L_x} \sin^2\frac{m\pi y_j}{L_y}\right) \times \left\{\frac{1}{j_{\max}} \sum_j [(\tilde{u}'_j)^2 + (\tilde{v}'_j)^2]\right\} \tag{23}$$

where the term in braces is identified with the right-hand side of (10), the variance (σ^2) of the fitted velocity to the data sample.

The vector distribution shown in Fig. 1 was obtained from sequential NOAA-6 AVHRR (11 micron band) images taken over a 23.6 hour interval on 20–21 May 1981 (Vastano and Borders, 1984). The images encompass a geographic region slightly larger than the area defined by 38–44°N, 144–150°E. The central feature is a semipermanent anticyclonic eddy between the First and Second Oyashio Intrusions located southeast of the Japanese island of Hokkaido. The sample of the flow field is comprised of 115 vector estimates of advective motion within the eddy, along the thermal ridge of the Oyashio Front, and within the Tohoku mixing zone to the south. A sequence of numerical experiments were carried out in which the order of the trigonometric basis functions was increased. The variance σ^2 steadily decreased with ascending orders and asymptotically approached a limiting value. This limiting variance is a measure of the departure of the velocity data sample from geostrophy. Figure 2 presents a scatter plot of observed versus calculated velocity components derived from a streamfunction expansion of seventh order in north and east basis functions and has an associated σ^2 of 10.1 cm^2 s^{-2} and a goodness of fit (r^2) of 0.81. The computed topographic relief for this approximation is shown in Fig. 3. The dimensions of the rectangular outline are slightly smaller than the fitted region chosen to include the vector distribution (L_x = 446 km, L_y = 362 km). The expected MSD for the topography values evaluated from (23) is 0.30 cm; this is a measure of experimental repeatability and not a measure of error. The central anticyclonic eddy has an excursion slightly greater than +20 cm, indicating a topographic dome relative to a −15 cm contour to the north across the thermal ridge. Altimeter ocean-surface topography profiles over warm core eddies are not available for the northwestern Pacific. However, using Seasat altimetry, Marsh *et al.* (1982) found that high mesoscale variability is present in the geographic region containing the warm core eddy and gives a range of rms surface height variability of 16–22 cm. The satellite topographic relief does correspond well to that found by Cheney and Marsh (1981) for warm core rings generated by the Gulf Stream in the North American

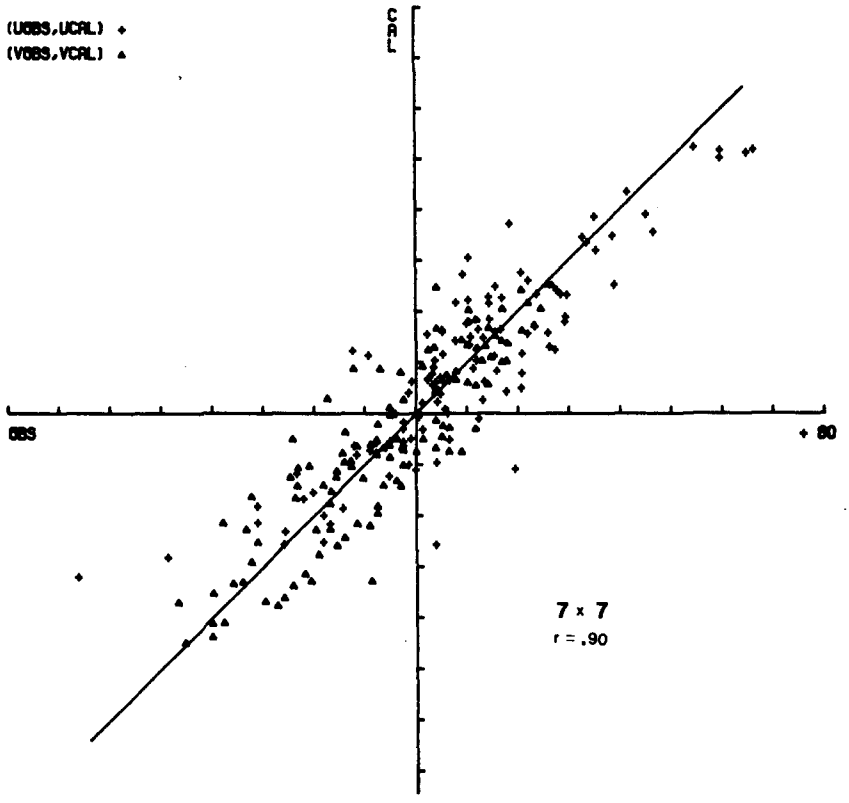

FIG. 2. Scatter plot of observed vs calculated velocity components (cm s^{-1}). Observed values are those obtained from the sequential images. Calculated values are computed from the streamfunction.

Slope Water region. A series of Seasat altimeter passes that intercepted warm core rings showed domes ranging from 75 (pass 277-A) to 45 (pass 486-D) cm relative to background. A single XBT measurement taken on 15 May 1981 in the anticyclonic eddy of Fig. 1 showed subarctic waters (<4°C) below 100 m depth and warm water (>10°C) at the surface (Vastano and Bernstein, 1984). This shallow temperature perturbation relative to the environment suggests that a smaller topographic range should be expected in comparison to the North Atlantic rings sampled by Seasat and indicates that the topography shown in Fig. 3 gives a reasonable estimate of the sea surface variation.

The sea surface topography or streamfunction contours over the warm core eddy in Fig. 1 show a nearly circular and symmetric field that represents a horizontally nondivergent approximation of the local flow pattern. Interest in the perturbations from a circular mean state and eddy azimuthal structure (Olson and Spence, 1978; Mied *et al.* 1983; McCalpin, 1984) has been generated by their evident relation to eddy instabilities and the availability of high spatial resolution field experiments and numerical models. While these investigations used field data in the form of temperature maps and numerically computed layer heights, Olson (1980) discussed the relevance of horizontal potential vorticity gradients to the baroclinic instability of mesoscale eddies. Vertical hydrographic sections were utilized since shipboard sampling limitations do not permit quasi-synoptic horizontal maps of vorticity. A further example of the quantitative information derivable from satellite flow estimates can be given by extracting the horizontal surface distribution of a local rotational property from the vector field in Fig. 1. This property is estimated by considering the quantity $Q = \nabla^2\Psi - \gamma^2\Psi$ which, in the context of geostrophic flow, is proportional to the perturbation potential vorticity defined by Gill (1982). The term Q is expressed in the vertical normal mode form where γ is the inverse of the radius of deformation for the first baroclinic eigenmode. The property $Q + \beta y$ is approximately conserved following a fluid parcel where β is df/dy. Hydrographic data were not taken over the eddy in the May 1981 period and the radius of deformation (40 km) was established on the basis of historical vertical sections of warm core eddies in the region (Tomosada, 1975). Figure 4 presents contours of $Q(10^7)$ s^{-1} overlayed on the vector distribution. The Q field near the

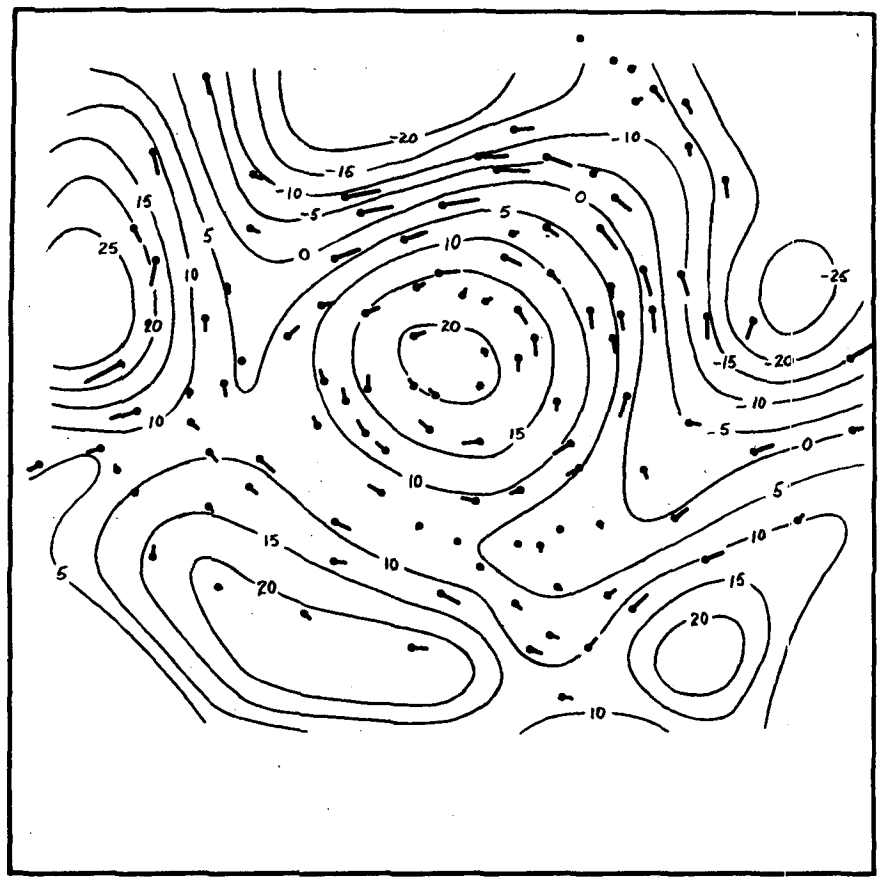

FIG. 3. Sea surface topography (cm) computed with the least-squares method overlayed on the velocity vectors shown in Fig. 1. Dots are placed at the tail of each vector.

center shows closed negative (anticyclonic) contours over the eddy with high values skewed to the western side and a broad, low value region extending to the northeast. There are no synoptic surface acquired vorticity maps for comparison to Fig. 4. Olson (1980) has given a zonal potential vorticity section that bisects a cyclonic eddy and shows slight departures from radial symmetry. Numerical experiments such as those reported by Smith and O'Brien (1983) have shown tongues of eddylike vorticity advected around eddies that have shapes similar to the northeastern extension of the eddy in Fig. 4. The Q field does have shape, magnitudes and features over the eddy that are reasonable in terms of previous results. The values near the edge of the map and the closure of the outlying features must be regarded as artifacts of the analysis procedure that imposes a zero streamfunction value at the boundaries.

3. Discussion

The topography in Fig. 3 is an estimate of the sea surface distribution to within the constant of integration in (17). Information about the mesoscale motion is present, since flow estimates are obtained from derivatives of this scalar field. The integration constant can be evaluated by computing dynamic heights from hydrographic stations or by microwave satellite observations. The primary disadvantage in the implementation of this method is the necessity for cloud-free views of the sea surface. Active microwave sensing of the sea surface such as that obtained by Seasat provides topographic information that is relatively free of this problem; yet its application to mesoscale studies is hampered by narrow (3 km) sensor footprints and temporal resolution. Movement of oceanic features and those orbital repetition rates that produce "gappy" data will result in aliasing for mesoscale interpretations of the altimetric data. In addition, the precision of altimeters is presently approximately 10 cm, a figure considerably larger than the attainable experimental repeatability of the least-squares method. The altimeter error in derived topography will be reduced with better geoid definition and a combination of the least-squares method and altimetric observation is clearly indicated.

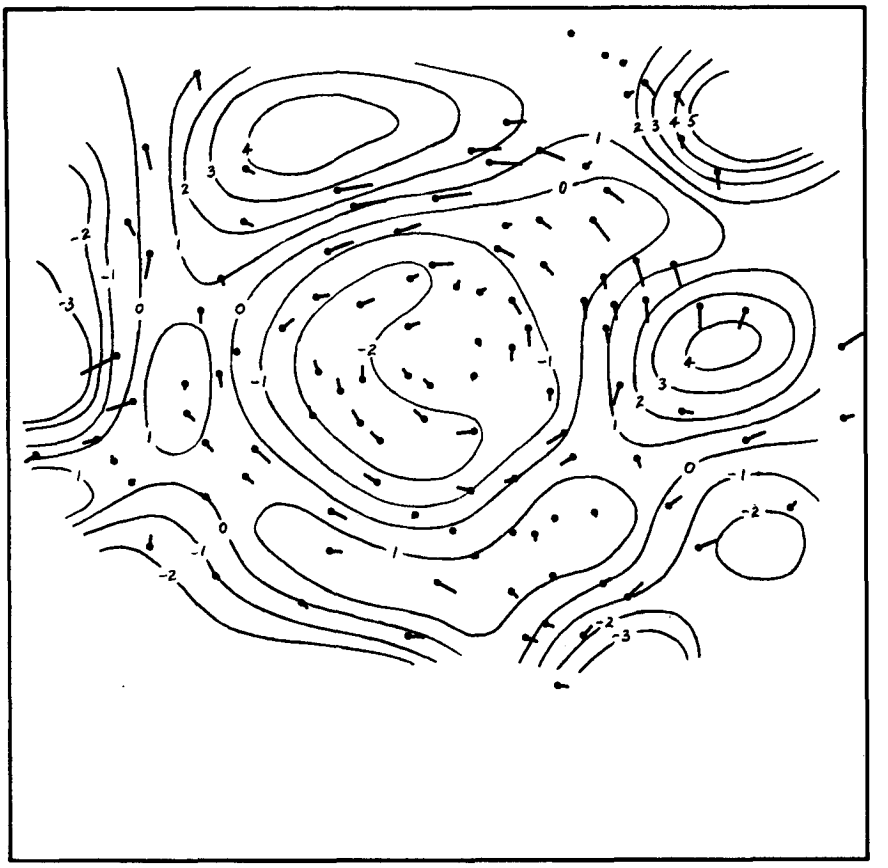

FIG. 4. Perturbation vorticity property $Q(10^7)$ s^{-1} computed from streamfunction and overlayed on the velocity vectors shown in Fig. 1.

The application of the least-squares method provides mesoscale flow fields that have areal coverage sufficient to define the sea surface expressions of individual mesoscale features and surroundings with temporal resolution at possible half-day intervals. This information can supplement data gathered in field experiments by surface platforms and can significantly enhance their interpretation. In fact, velocity estimate sources other than infrared imagery such as hydrography, drifters, GEK observations, visible imagery and radar altimetry can be included to provide data sets for the least-squares method. The topographic fields or derivative velocity fields present the opportunity to initialize and verify mesoscale computer models and can be employed alone for local forecasts of environmental flow conditions. As an example of an extension of the method, the velocity vector fields can be combined with coincident, accurate sea surface temperature maps of similar resolution such as those derived from satellite data with corrections for atmospheric cloud and water vapor effects (Bernstein, 1982; Vastano and Bernstein, 1984). The combination will provide estimates of the total time rate of change of surface temperature and advective flow for studies of the local time rate of change of temperature in mesoscale fields and will be applicable to heat content studies of the oceanic surface layer.

Acknowledgments. The image processing was carried out at the Satellite-Oceanography Facility, Scripps Institution of Oceanography, La Jolla, California. The authors thank Robert Whritner for assistance in archiving the images of the Oyashio Front and Koren Abdullah for help in the flow field analysis. Andrew Vastano was supported by Grant OCE 80-26037 of the National Science Foundation and the Office of Naval Research under Contract N00014-75-0537.

REFERENCES

Bernstein, R. L., 1982: Sea surface temperature estimation using the NOAA-6 satellite AVHRR radiometer. *J. Geophys. Res.*, **87**, 9455–9465.

Cheney, R. E., and J. G. Marsh, 1981: Seasat altimeter observations of dynamic topography in the Gulf Stream region. *J. Geophys. Res.*, **86**, 473–483.

Gill, A. E., 1982: *Atmosphere-Ocean Dynamics.* Academic Press, 662 pp.

Hubertz, J. M., A. W. Garcia and R. O. Reid, 1972: Objective analysis of oceanic surface currents. *Contributions on the Physical Oceanography of the Gulf of Mexico.* Gulf Publishing Company, 139–148.

Marsh, J. G., R. E. Cheney, T. V. Martin and J. J. McCarthy, 1982: Mean sea surface computations in the Northwest Pacific based upon satellite altimeter data. Unpublished Report, General Meeting: Int. Assoc. Geodesy, Tokyo, Japan, 8 pp.

McCalpin, J. D., 1984: Analysis of azimuthal mode dynamics of mesoscale eddies. M.S. thesis, Texas A&M University, 72 pp.

McWilliams, J. C., 1976: Maps from the Mid-Ocean Dynamics Experiment: Part I: Geostrophic streamfunction. *J. Phys. Oceanogr.*, **6,** 810–826.

Meid, R. P., G. J. Lindemann and J. M. Bergin. 1983: Azimuthal structure of a cyclonic Gulf Stream ring. *J. Geophys. Res.*, **88,** 2530–2546.

Olson, D. B., 1980: The physical oceanography of two rings observed by the Cyclonic Ring Experiment. Part II: Dynamics. *J. Phys. Oceanogr.*, **10,** 514–528.

——, and T. W. Spence, 1978: Asymmetric disturbances in the frontal zone of a Gulf Stream ring. *J. Geophys. Res.*, **83,** 4691–4696.

Pritchard, D. W., 1948: Streamlines from a discrete vector field: With application to ocean currents. *J. Mar. Res.*, **3,** 296–303.

Smith, D. C., and J. J. O'Brien, 1983: The interaction of a two-layer isolated mesoscale eddy with bottom topography. *J. Phys. Oceanogr.*, **13,** 1681–1697.

Tomosada, A., 1975: Observations of a warm eddy detached from the Kuroshio east of Japan. *Bull. Tokai Reg. Fish Res. Lab.*, **81,** 13–85.

Vastano, A. C., and R. L. Bernstein, 1984: Mesoscale features along the First Oyashio Intrusion. *J. Geophys. Res.*, **89,** 587–596.

——, and S. E. Borders, 1984: Sea surface motion over an anticyclonic eddy on the Oyashio Front. *Remote Sens. Environ.*, **16,** 87–90.